Research Article

Joko Waluyo*, Farida Dwi Rahmawati, Muhammad Ghozy Izzulhaq, Ibnu Tryansar Purba, Mujtahid Kaavessina, Wusana Agung Wibowo, Sunu Herwi Pranolo, Haris Puspito Buwono, Ardie Septian, and Muflih Arisa Adnan

A comparative analysis of single-step and multi-step methods for producing magnetic activated carbon from palm kernel shells: Adsorption of methyl orange dye

https://doi.org/10.1515/gps-2024-0234
received November 05, 2024; accepted February 25, 2025

Abstract: Synthetic dyes in wastewater present a challenging problem that requires special attention due to the high environmental risks, and magnetic adsorbents appear as promising alternatives to solve it. Magnetic activated carbons (MAC) were prepared by comparing single- and multi-step methods. Palm kernel shells were used as precursors, activated with $ZnCl_2$, and then magnetized by adding a solution containing Fe^{3+} ions ($FeCl_3$). Iron compound inclusion aims to enhance the effectiveness of activated carbon as an adsorbent for liquid waste. Fourier transform infra-red characterization showed that the functional groups detected on the activated carbon and MAC were O–H, C═O, C═C, C≡N, and C–O. The effect of preparation methods and dye concentration (10–30 $mg{\cdot}L^{-1}$) on adsorption and kinetics were investigated. Characterization showed that MAC prepared through multi-step pyrolysis (M-MAC) has larger pores, achieving an adsorption capacity of up to 6.953 $mg{\cdot}g^{-1}$ with a 28% dye removal efficiency, making it superior in adsorption performance. Furthermore, the adsorption data fitted well with the Redlich–Peterson isotherm model with R^2 = 0.9788 for M-MAC, while the adsorption kinetics agreed well with both the pseudo-first-order and pseudo-second-order models. Moreover, NaOH successfully recovered MAC with desorption efficiencies of up to 98.34%.

Keywords: dye adsorption, isotherm adsorption, kinetic adsorption, magnetic activated carbon, methyl orange

1 Introduction

Industrial growth has driven global economic development but also caused significant environmental harm. The textile industry, in particular, contributes heavily to pollution through its wastewater, which contains 10–200 $mg{\cdot}L^{-1}$ of dyes and chemical additives. Shockingly, about 90% of these dyes are discharged into rivers without proper degradation, even after treatment, underscoring the need for better wastewater management [1]. Synthetic dyes in wastewater, such as methyl orange (MO), pose significant environmental risks due to their stability and resistance to degradation [2]. MO, widely used in textiles, printing, and paper industries, contains azo bonds that make it highly resistant to biological treatments, leading to its persistence in aquatic systems [3]. MO-laden wastewater is toxic and highly colored [4], harming aquatic ecosystems and complicating compliance with environmental standards. Conventional methods like coagulation, flocculation, and biological processes often fail to fully remove MO, highlighting the need for advanced remediation techniques. Among treatment methods, adsorption stands out for its simplicity, cost-effectiveness, small space requirement, and high efficiency [5].

Various adsorbents such as biochar, activated carbon, carbon nanotubes, zeolites, clay minerals, and others have

* **Corresponding author: Joko Waluyo**, Chemical Engineering Department, Universitas Sebelas Maret, Surakarta, 57126, Indonesia, e-mail: jokowaluyo@staff.uns.ac.id
Farida Dwi Rahmawati, Muhammad Ghozy Izzulhaq, Ibnu Tryansar Purba, Mujtahid Kaavessina, Wusana Agung Wibowo, Sunu Herwi Pranolo: Chemical Engineering Department, Universitas Sebelas Maret, Surakarta, 57126, Indonesia
Haris Puspito Buwono: Chemical Engineering Department, Politeknik Negeri Malang, Malang, 65141, Indonesia
Ardie Septian: Research Center for Environmental and Clean Technology, Badan Riset dan Inovasi Nasional, Serpong, 15314, Indonesia
Muflih Arisa Adnan: Department of Chemical Engineering, Islamic University of Indonesia, Sleman, Daerah Istimewa Yogyakarta, 55584, Indonesia

been used for dye waste adsorption [6]. Activated carbon (AC) is a frequently used adsorbent due to its large surface area, good chemical resistance, and thermal stability [7]. Furthermore, the application of magnetic technology to AC producing magnetic activated carbon (MAC) becomes a next-step development on adsorption capacity, which combines the adsorptive properties of AC with the ease of separation using a magnetic field [8–12]. Research has shown that AC can be made from various types of biomass precursors, including rape straw powder [13], coffee grounds [14], peanut shells [7], furfural residues [15], and more. Palm kernel shell (PKS) is also a potential biomass for making AC [16–18]. Indonesia, a leading global palm oil producer, has an estimated 15 million hectares of palm oil plantations and produces 49.1 million tons of crude palm oil annually [19]. The average yield across plantations is approximately 13.8 tons of fresh fruit bunches (FFB) per hectare per year [20]. PKS, a byproduct constituting 6–7% of FFB in the palm oil industry [21], holds significant potential for sustainable AC production due to its fixed carbon content of 18.89–19.57 wt% [22,23].

MAC generally has a lower specific surface area than AC due to the presence of Fe ions in its precursor (997 $m^2 \cdot g^{-1}$ vs 1,198 $m^2 \cdot g^{-1}$), corresponding to reduced pore volume (0.79 $cm^3 \cdot g^{-1}$ vs 0.97 $cm^3 \cdot g^{-1}$) and adsorption capacity (195 $mg \cdot g^{-1}$ vs 259 $mg \cdot g^{-1}$) [24]. However, MAC's magnetic properties enable easy separation from solutions, enhancing its reusability and efficiency across multiple adsorption cycles [10,25]. Its removal efficiency for MO consistently exceeds 90% even after five regeneration cycles, demonstrating remarkable durability [24]. The slight decline in performance is likely due to the accumulation of residual MO molecules and their intermediates in MAC's pores [24]. Moreover, MAC can be synthesized from low-cost, sustainable materials, making it an eco-friendly option for water treatment [26]. MAC production involves two main methods: single-step and multi-step pyrolysis. Both methods involve activation and magnetization processes. In the multi-step method, biomass undergoes carbonization and activation via pyrolysis to remove volatile compounds, followed by magnetization. This method offers better control over the final product properties but is more time- and resource-intensive [16]. On the other hand, the single-step method combines carbonization and magnetization in a single stage, which is more efficient in terms of time and cost but sometimes produces products with less optimal porosity and surface area [5].

The multi-step pyrolysis method has been shown to produce high-quality MAC with excellent adsorption properties. For instance, one study used pineapple leaves as a biomass precursor and KOH and Fe_3O_4 as activating agents, achieving a pore volume of 0.1098 [27]. Another study utilized lignin and $FeSO_4$ as impregnation agents, demonstrating that the resulting MAC had an adsorption capacity of 69.80 mg-P·g^{-1} and could remove 84.65% and 96.97% of total phosphorus from filtered raw and treated domestic wastewater, respectively [28]. These findings highlight the effectiveness of the multi-step method in producing MAC with strong adsorption performance for various applications. The two-step method offers the benefit of significantly increasing the carbon content. During the initial pyrolysis stage, a foundational porosity is established, which is subsequently refined and expanded through chemical activation [29], although it requires more time and resources.

NaOH was preferred over other regeneration chemical agents due to its unique properties and proven efficacy in desorption processes. Its strong alkaline nature enables efficient breaking of specific bonds (e.g., hydrogen bonds or electrostatic interactions) between adsorbates and adsorbents, which is critical for effective regeneration. Additionally, NaOH is cost-effective, readily available, and generates less environmental impact compared to other reagents like organic solvents or strong acids, which may pose handling, safety, or disposal challenges [30]. Furthermore, its use is well-supported by previous studies for desorbing pollutants and organic compounds, e.g., dyes, heavy metals, and pharmaceutical waste [31–33], which has demonstrated superior regeneration performance in adsorption–desorption systems.

This study focuses on the production of MAC from PKS, utilizing two chemical activation approaches with $ZnCl_2$ and $FeCl_3$ as activation agents. The research aims to compare the effectiveness of these methods in generating MAC, while also examining its performance through detailed isotherm and kinetic analyses. Furthermore, the investigation includes a regeneration process using NaOH to assess the material's ability to recover and maintain its functional properties for potential reuse in various applications.

2 Materials and methods

2.1 Materials

The primary source material comprised PKS from PT Kayan Lestari's oil palm plantations (East Kalimantan). The chemical components utilized in the investigation encompassed $ZnCl_2$ (98%, Sigma Aldrich) as an activator and HCl (37%, Sigma Aldrich) for demineralization of water. In the creation of magnetic carbon, $FeCl_3.6H_2O$

(97%, Sigma Aldrich) was employed in the synthesis of iron oxide. Moreover, the adsorption analysis incorporated MO (85%, Sigma Aldrich) and NaOH (98%, Sigma Aldrich) also used as regenerating agents.

2.2 Preparation of MAC

The MAC was produced using either a single- or multi-step process with $FeCl_3$ serving as the magnetizing agent and $ZnCl_2$ as the activating agent. Initially, the PKS were ground to a 20-mesh size and cleaned to remove any impurities. The cleaned PKS were dried in an oven at 80°C for 12 h.

In the single-step method, the activation process is carried out once using $ZnCl_2$, $FeCl_3$, and $ZnCl_2/FeCl_3$ as the activator. Each activator was dissolved in 50 mL of distilled water and then mixed with 20 g of PKS according to the weight ratio specified in Table 1. The mixture is stirred at 90°C for 1.5 h, then filtered and dried in an oven at 80°C for 8 h. The activated PKS was then pyrolyzed in a furnace at 600°C for 1 h. The resulting MACs were soaked in a 0.1 mol·L^{-1} HCl solution for 12 h to remove minerals [34]. They were rinsed and dried to produce $ZnCl_2$-AC (Z-AC), $FeCl_3$-magnetized biochar (F-MC), and $ZnCl_2/FeCl_3$ one-step magnetic AC (O-MAC).

In the multi-step method, activation was conducted twice on $ZnCl_2$ and $FeCl_3$. The Z-AC product from the first activation is mixed with 50 mL of $FeCl_3$ solution (PKS:$FeCl_3$ = 1.0:1.0). The second activation was performed for 1.5 h at 90°C, followed by a second round of pyrolysis in the furnace under the same conditions as the initial pyrolysis. The MAC was then soaked in an HCl solution for 12 h for demineralization. The sample then rinsed to neutrality and dried to yield $ZnCl_2/FeCl_3$ multi MAC (M-MAC).

2.3 Characterization

The O-MAC, M-MAC, Z-AC, and F-MC were evaluated using scanning electron microscope (SEM) analysis to determine their morphological structure at magnifications of 2,000×. Fourier transfer infra-red (FTIR) analysis was also conducted to identify the functional groups in the MAC. Additionally, X-ray diffraction (XRD) analysis was used to identify the presence of Fe^{3+} compounds successfully synthesized in the MAC. Surface physical analysis using the Brunauer–Emmett–Teller (BET) method was employed to determine the typical isotherm adsorption.

Table 1: Activator composition

Sample	Weight ratio
O-MAC	PKS:$ZnCl_2$:$FeCl_3$ = 1.0:1.5:1.0
M-MAC	PKS:$ZnCl_2$ = 1.0:1.5
Z-AC	PKS:$ZnCl_2$ = 1.0:1.0
F-MC	PKS:$FeCl_3$ = 1.0:1.0

2.4 Application in MO absorption

The adsorption capacity of the four AC samples was tested using MO solution. Adsorption happens due to the surface area of the adsorbent; a larger available surface area allows more molecules to be absorbed [35]. This process was carried out using 1 g·L^{-1} of AC in MO solutions with concentrations of 10–30 mg·L^{-1}. The absorbance of the MO solution before and after adsorption was measured using a UV-Vis spectrophotometer at a maximum wavelength of 464 nm [14]. The adsorption capacity and the percentage of compound removal by the adsorbent can be calculated using Eqs. 1 and 2.

$$q_e = V(\mathrm{Co} - \mathrm{Ce})/m \quad (1)$$

$$\%\ \text{removal} = (\mathrm{Co} - \mathrm{Ce})/\mathrm{Co} \times 100\% \quad (2)$$

Furthermore, the adsorption testing was divided into two parts: isotherm and kinetics. These tests aim to determine the appropriate kinetic and isotherm models. The isotherm adsorption test began by preparing MO solutions with varying concentrations of 10–30 mg·L^{-1}. Then, 50 mg of each sample was added to each MO prepared solution. The mixtures were left to stand for 24 h at ambient conditions, after which the AC was separated from the solution. A UV-Vis spectrophotometer was used to measure the absorbance (concentration) of the MO solution before and after the adsorption process.

Several models used to model adsorption, including the Langmuir, Freundlich, Temkin, and Redlich-Peterson models. The Langmuir model describes adsorption as the formation of a monolayer on a homogeneous adsorbent surface. In contrast, the Freundlich model indicates adsorption on a heterogeneous adsorbent surface with multilayer formation and varying adsorption energies. The Temkin model considers interactions between adsorbent and adsorbate and a uniform distribution of adsorption energy on the adsorbent surface, suitable for intermediate concentrations. The Redlich-Peterson model combines aspects of both the Freundlich and Langmuir isotherms, incorporating linear and exponential components of the adsorption process with three parameters. This model can be applied to both homogeneous and heterogeneous adsorbent surfaces. Each isotherm model can be determined using Eq. 3 (Langmuir),

Eq. 4 (Freundlich), Eq. 5 (Temkin), and Eq. 6 (Redlich-Peterson) [36].

$$q_e = q_m \times k_L \times Ce/(1 + k_L \times Ce) \quad (3)$$

$$q_e = K_F \times Ce^{1/n} \quad (4)$$

$$q_e = (RT/bT)\ln(K_T \times Ce) \quad (5)$$

$$q_e = K_R \times Ce/(1 + a_R \times Ce^g) \quad (6)$$

The kinetics of adsorption were tested by varying the contact time (0–180 min). The solution samples were taken at predetermined time intervals and their absorbance was measured using a UV-Vis spectrophotometer. The kinetic models, which have been extensively studied, can be determined using Eq. 7 (pseudo first order) and Eq. 8 (pseudo second order) [37].

$$1/Q_t = (k_1/Q_1) \times (1/t) + 1/Q_1 \quad (7)$$

$$1/Q_t = (1/k_2Q_1) \times (t/Q_2) \quad (8)$$

2.5 Regeneration and reuse study

The regeneration process began with drying the used AC in an oven at 105°C for 8 h to achieve a consistent moisture content. Subsequently, the dried AC was immersed in a regenerating agent solution and stirred at 150 rpm for 2 h at room temperature (30°C) to facilitate the desorption of adsorbed contaminants. The treated AC was then separated from the solution, thoroughly washed with distilled water to remove residual regenerating agents, and subjected to a second drying cycle at 105°C for 8 h. Once dried, the regenerated AC was prepared for reuse in subsequent adsorption cycles. In this trial, NaOH was used as the regenerating agent with varying concentrations of 0.5 and 1 mol·L^{-1} to evaluate its effectiveness in regenerating the AC. The regeneration capability is measured based on the % desorption calculated using Eq. 9.

$$\%\ \text{desorption} = Ce_{Desorption}/Ce_{Adsorption} \times 100\% \quad (9)$$

3 Results and discussion

3.1 Characterization of O-MAC, M-MAC, Z-AC, and F-MC

3.1.1 SEM

The SEM magnification revealed the morphology of each sample at 2,000× (Figure 1). The M-MAC exhibits more surface cavities compared to the other samples. Furthermore, the pore distribution in M-MAC is more uniform, leading to better porosity. Conversely, O-MAC, Z-AC, and F-MC display

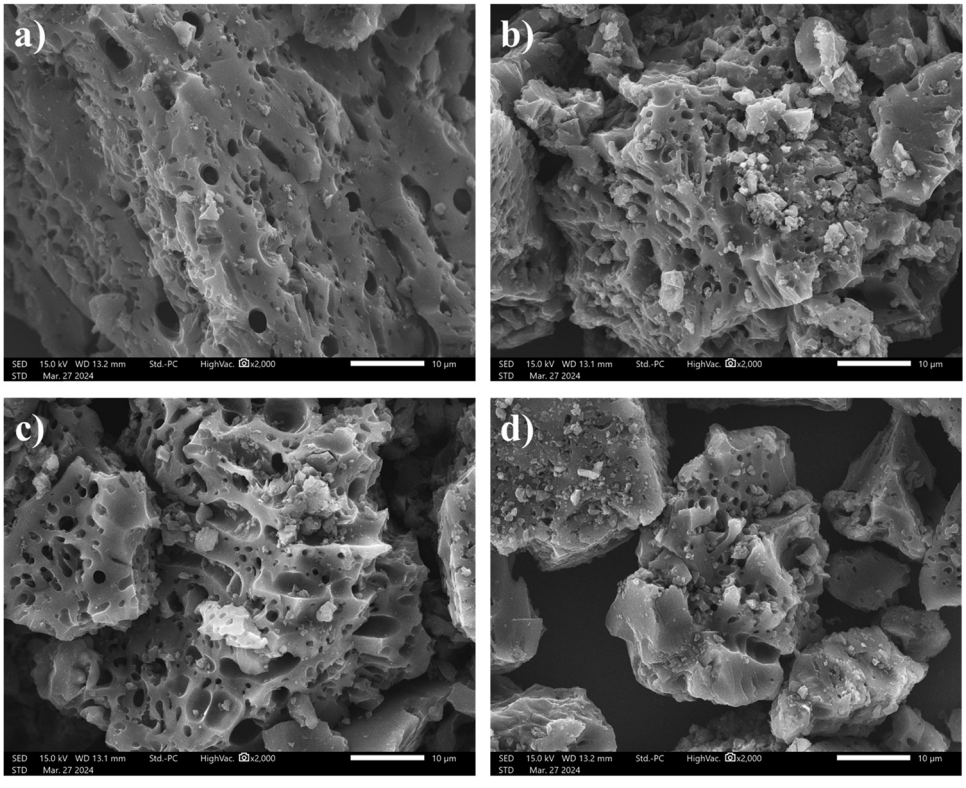

Figure 1: Analysis SEM: (a) O-MAC; (b) M-MAC; (c) Z-AC; and (d) F-MC at 2,000× magnification.

a looser surface morphology (with void spaces). This finding indicates that the morphology of PKS activated using the multi-step method with $ZnCl_2$ and $FeCl_3$ activators has larger and more uniformly distributed pores compared to the single-step method.

3.1.2 FTIR and XRD

Figure 2 displays the FTIR spectra of AC that has undergone different treatments, including activation and a combination of activation with magnetization. Each FTIR spectrum curve showed absorbance peaks at specific wavelengths, indicating the presence of particular chemical bonds within the AC structure. All four samples exhibit significant peaks at several wavelength regions, suggesting similarities in their basic chemical composition, although variations due to the applied treatments are evident.

The analysis reveals that all four samples share a common peak at 1,624 cm^{-1}, which indicates the presence of C═C bonds. Additionally, O–H bonds were found in the wavelength range of 3,600–3,200 cm^{-1}, typically present in hydroxyl groups. The presence of these hydrogen bonds suggests that all samples have good adsorption potential. C≡N bonds were also detected in the range of 2,210–2,280 cm^{-1}, further indicating the presence of various functional groups in the AC samples. The analysis results also show the presence of C–O bonds in the F-MC sample and C═H bonds in the O-MAC sample. These bonds reflect that the activation and magnetization treatments have successfully modified the surface chemical structure of the AC, which can influence its adsorption properties.

The XRD diffraction patterns of O-MAC, M-MAC, Z-AC, and F-MC are shown in Figure 3. The presence of broad diffraction peaks indicates that the MAC has undergone a structural transformation from an organic crystal to a more refined graphite-like crystalline structure. In these XRD results, one of the diffraction peaks appears around 30.93° for O-MAC, 35.45° for M-MAC, 36.70° for Z-AC, and 36.50° for F-MC. This suggests the potential presence of iron-based compounds, particularly Fe_3O_4 (magnetite). These peaks align with the standard diffraction pattern for magnetite, as listed in the Joint Committee on Powder Diffraction Standards card No. 19-0629, with characteristic Fe_3O_4 peaks appearing at 2θ = 30.1°, 35.4°, 43.1°, 57.0°, and 62.5° corresponding to the reflections from the (211), (311), (400), (511), and (440) [38].

The identification of XRD peaks on M-MAC and O-MAC indicated that the MAC was successfully synthesized. The magnetic properties of Fe_3O_4 allow the MAC to be easily separated from the mixture after the adsorption process. However, the use of $FeCl_3$ as the magnetizing agent in this study may have limited the magnetic properties of the AC, the result plotted in this study is relatively similar to previous findings [39]. Other studies exhibited better quality; they have a much stronger peak on their sample characteristic which is prepared utilizing F_3O_4 for their magnetizing agent [40–42]. Higher peaks indicate stronger XRD intensity, meaning more crystals in the sample have the same interatomic spacing, giving the sample a uniform orientation and a more ordered structure.

3.1.3 Surface physical characteristics

Nitrogen adsorption–desorption isotherms (Figure 4a–d) reveal that all carbon-based samples show similar

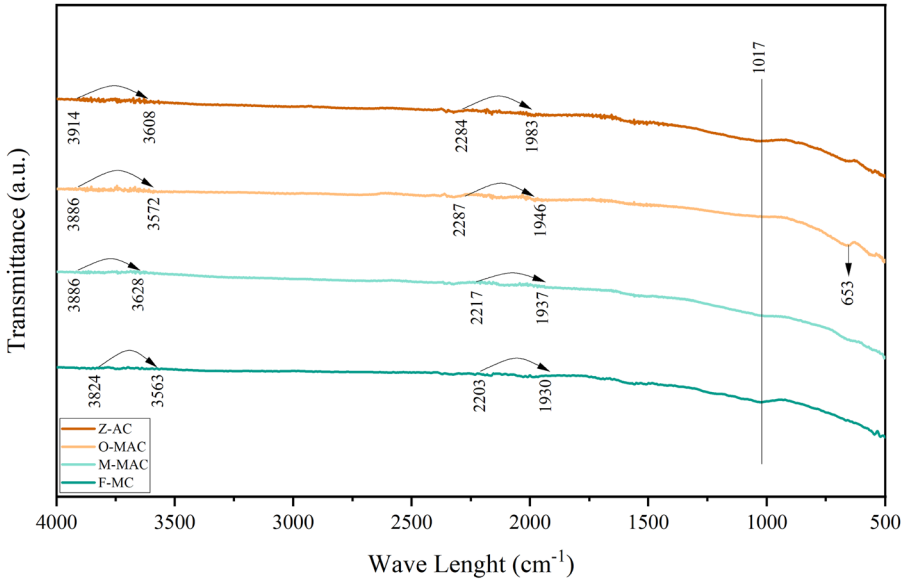

Figure 2: FTIR analysis.

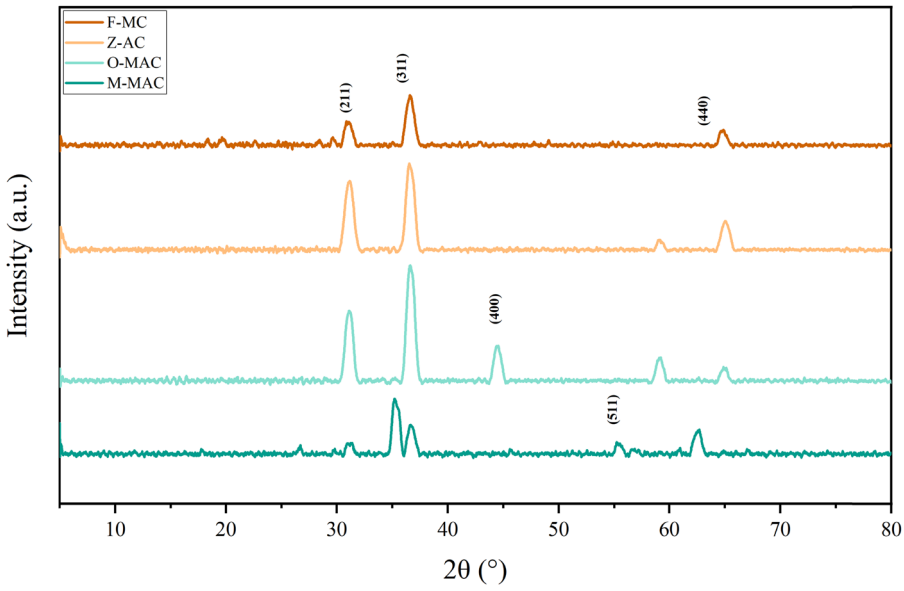

Figure 3: XRD analysis.

adsorption characteristics. These isotherms suggest a combination of microporous and mesoporous structures within the materials, as evidenced by the initial rapid increase in adsorbed nitrogen at low relative pressures, followed by a gradual rise at higher pressures. The shape of the isotherm is typically classified as Type IV with a hysteresis loop.

This type describes the adsorption behavior of specific mesoporous materials, characterized by pore

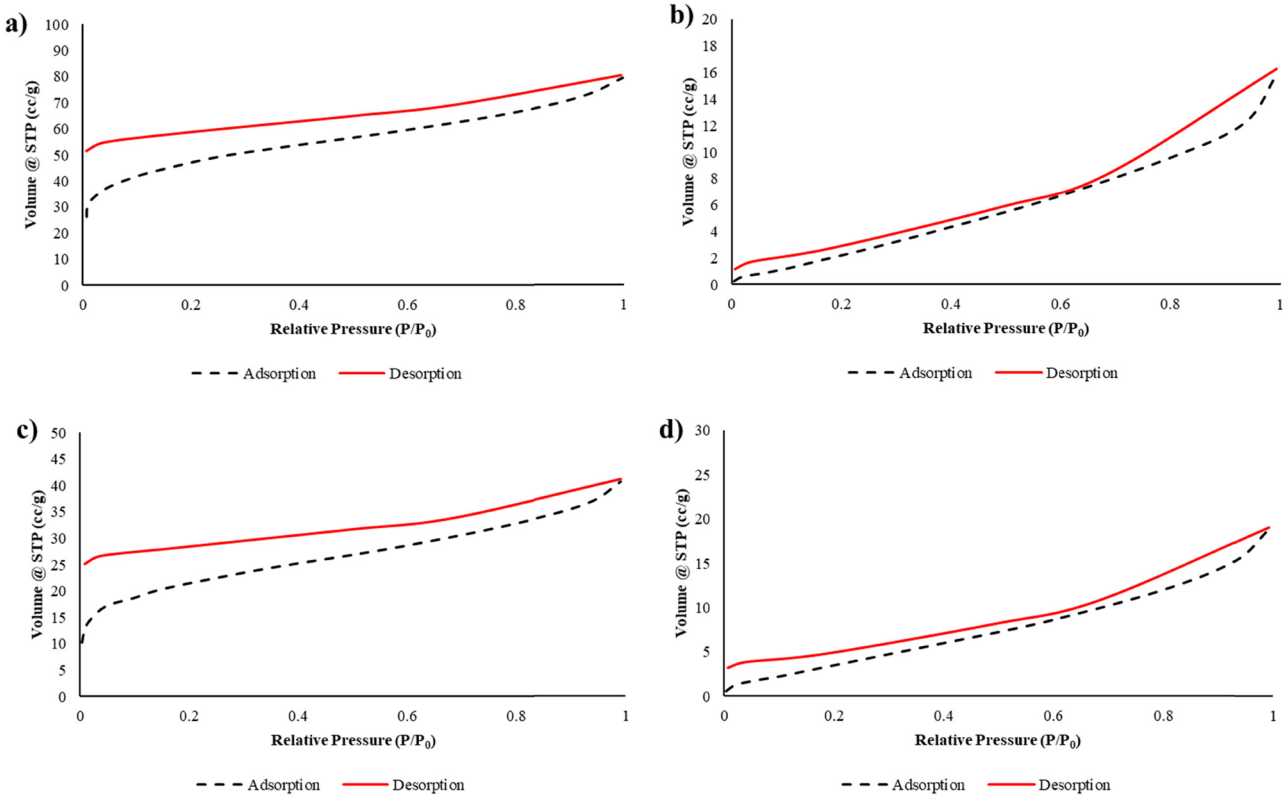

Figure 4: The adsorption–desorption isotherms of N2 at 77 K: (a) O-MAC; (b) M-MAC; (c) Z-AC; and (d) F-MC.

condensation and hysteresis between the desorption and adsorption branches [36], which is common in carbon materials with interconnected pores. This study has a finding similar to that in previous research based on adsorption and desorption of tectonically deformed coal [43].

The adsorption branch (dashed line) and desorption branch (solid line) show a noticeable hysteresis loop in each sample. This hysteresis loop, common in mesoporous materials, indicates capillary condensation within the pores. The wider the hysteresis loop, the larger the pore size distribution and volume, pointing to a material with a substantial mesoporous network [44]. Variations in the hysteresis loops across samples may reflect slight differences in pore connectivity or surface chemistry, which affects adsorption and desorption behavior.

3.2 Adsorption study on MO

3.2.1 Effect of MO initial concentration on adsorption capacity and MO removal

Adsorption of MO onto MAC occurs through various mechanisms, including mesopore filling, electrostatic forces, hydrogen bonding, n–π interactions, and π–π interactions. Hydrogen bonding involves interactions between hydroxyl groups present on the carbon surface and the oxygen or nitrogen atoms in MO. The n–π interaction arises from bonds such as O–H or oxygen-containing groups on the carbon surface interacting with the aromatic rings of MO. Similarly, π–π interactions occur between the π electrons in the aromatic structure of the carbon and those in MO's aromatic ring. An illustration of the adsorption process is provided in Figure 5.

This study was conducted using MAC at a concentration of 1 $g{\cdot}L^{-1}$ in MO solutions at concentrations of 10–30 $mg{\cdot}L^{-1}$. Figure 6 illustrates the adsorption capacity and removal efficiency for MO. Among the tested materials, M-MAC demonstrated superior performance. M-MAC and O-MAC exhibited the highest adsorption capacities of 6.953 and 3.312 $mg{\cdot}g^{-1}$, respectively, at 25 $mg{\cdot}L^{-1}$ MO. (Figure 6a and b). In contrast, Z-AC and F-MC exhibited significantly lower capacities of 1.191 and 1.027 $mg{\cdot}g^{-1}$, respectively (15 $mg{\cdot}L^{-1}$ MO) (Figure 6c and d). Furthermore, it was observed that increasing the initial dye concentration enhances the adsorption capacity but reduces dye removal because it provides more dye molecules available to interact with the adsorbent's active sites [46]. However, at a certain moment, along with the increasing initial dye concentration, the number of available active sites becomes limited, as most sites have been occupied by dye molecules, thus reducing the adsorption capacity [6]. However, this can also reduce overall dye removal efficiency, as higher concentrations may lead to quicker saturation of available sites [47], increased competition among dye molecules for those sites [48,49], and potential kinetic limitations where the rate of diffusion to the adsorbent surface cannot keep up with the influx of dye [50,51]. According to Eq. 1, the adsorption capacity (q_e) is directly proportional to the difference in initial (Co) and

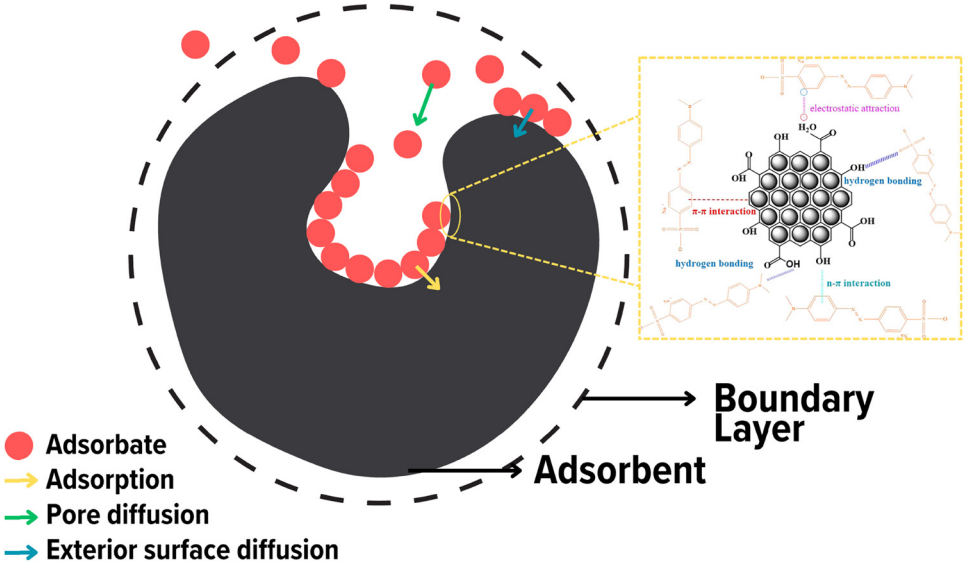

Figure 5: Mechanism of MO adsorption on MAC. Reprinted with permission from Elsevier [45].

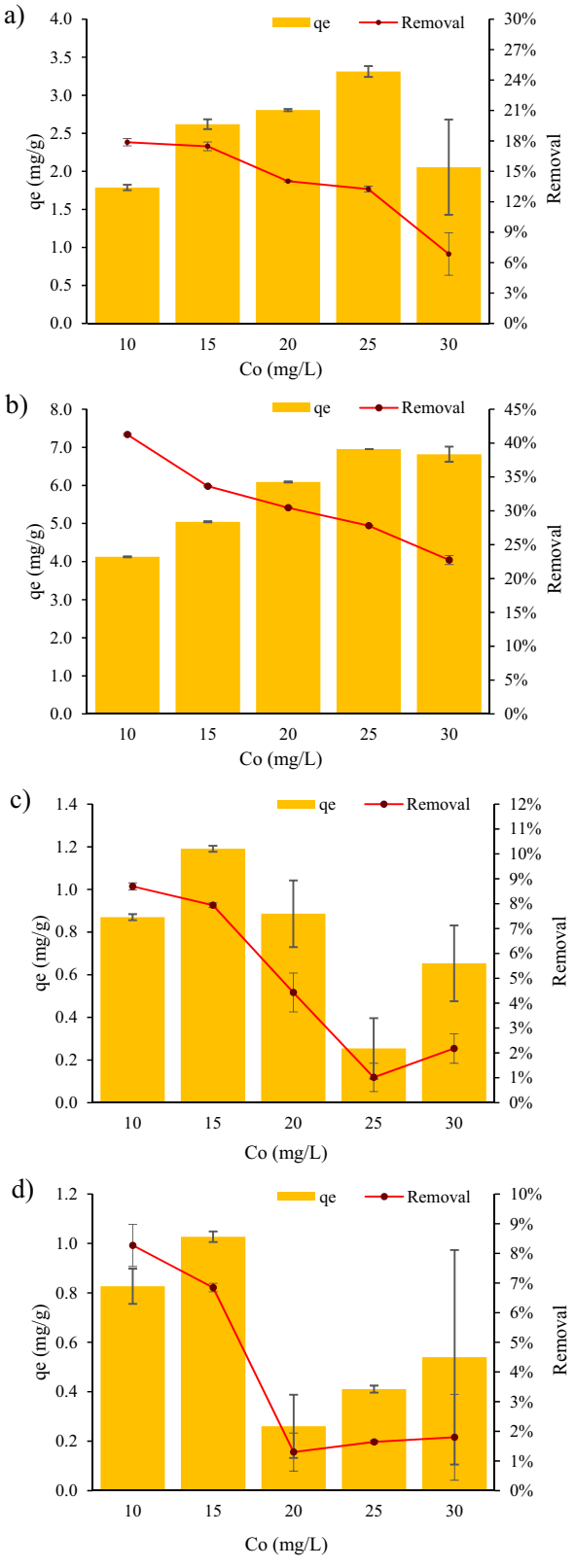

Figure 6: Effect of MO concentration on adsorption capacity: (a) O-MAC; (b) M-MAC; (c) Z-AC; and (d) F-MC.

equilibrium (Ce) concentrations of the adsorbate. Using a higher Co can provide a greater concentration gradient, which typically enhances the adsorption process. Prior research has demonstrated that an increase in initial dye concentration leads to a higher adsorption capacity utilizing Osmanthus fragrans biomass charcoal. In an experimental study, various dyes were tested at different initial concentrations: malachite green (800 $mg{\cdot}L^{-1}$), Congo red (1,000 $mg{\cdot}L^{-1}$), rhodamine B (500 $mg{\cdot}L^{-1}$), MO (1,000 $mg{\cdot}L^{-1}$), methylene blue (700 $mg{\cdot}L^{-1}$), and crystal violet (500 $mg{\cdot}L^{-1}$). The adsorption capacities recorded for these dyes were 6,501.09, 2,870.30, 554.93, 6,277.72, 626.50, and 3,539.34 $mg{\cdot}g^{-1}$, respectively [52]. Additionally, concentration polarization can occur, creating a layer of concentrated dye near the adsorbent that reduces the effective concentration gradient driving further adsorption.

Fe-AC can exhibit a dual behavior depending on the manner in which iron is incorporated into the carbon matrix; on one hand, the addition of iron particles may lead to a reduction in adsorption capacity compared to regular AC due to physical blockage or partial coverage of pore sites, which diminishes the overall accessible surface area. This effect is exacerbated when the iron is poorly distributed or the particles are excessively large, leading to uneven pore obstruction. While on the other hand, the presence of iron can introduce additional adsorption sites through favorable chemical interactions with specific adsorbates, such as heavy metal ions, thereby potentially enhancing the adsorption capacity for certain pollutants.

3.2.2 Isotherm models

The adsorption isotherm analysis (Figures 7–10 and Table 2) revealed distinct interactions between MO and the synthesized adsorbents. Four models – Langmuir, Freundlich, Temkin, and Redlich-Peterson – were evaluated to elucidate the adsorption mechanisms. The Redlich-Peterson model demonstrated superior fitting for all samples, particularly M-MAC (R^2 = 0.9788), aligning with its hybrid nature that integrates monolayer (Langmuir) and heterogeneous multilayer (Freundlich) adsorption behaviors [53]. This model's three-parameter (Eq. 6) allows flexibility in describing complex surface interactions.

For M-MAC, the exponent g (0.597) deviated from unity, indicating heterogeneous adsorption, likely due to its mesoporous structure (Figure 1) and functional groups (Figure 2) that promote multilayer binding. Conversely, O-MAC's g (0.786) approached homogeneity, suggesting a

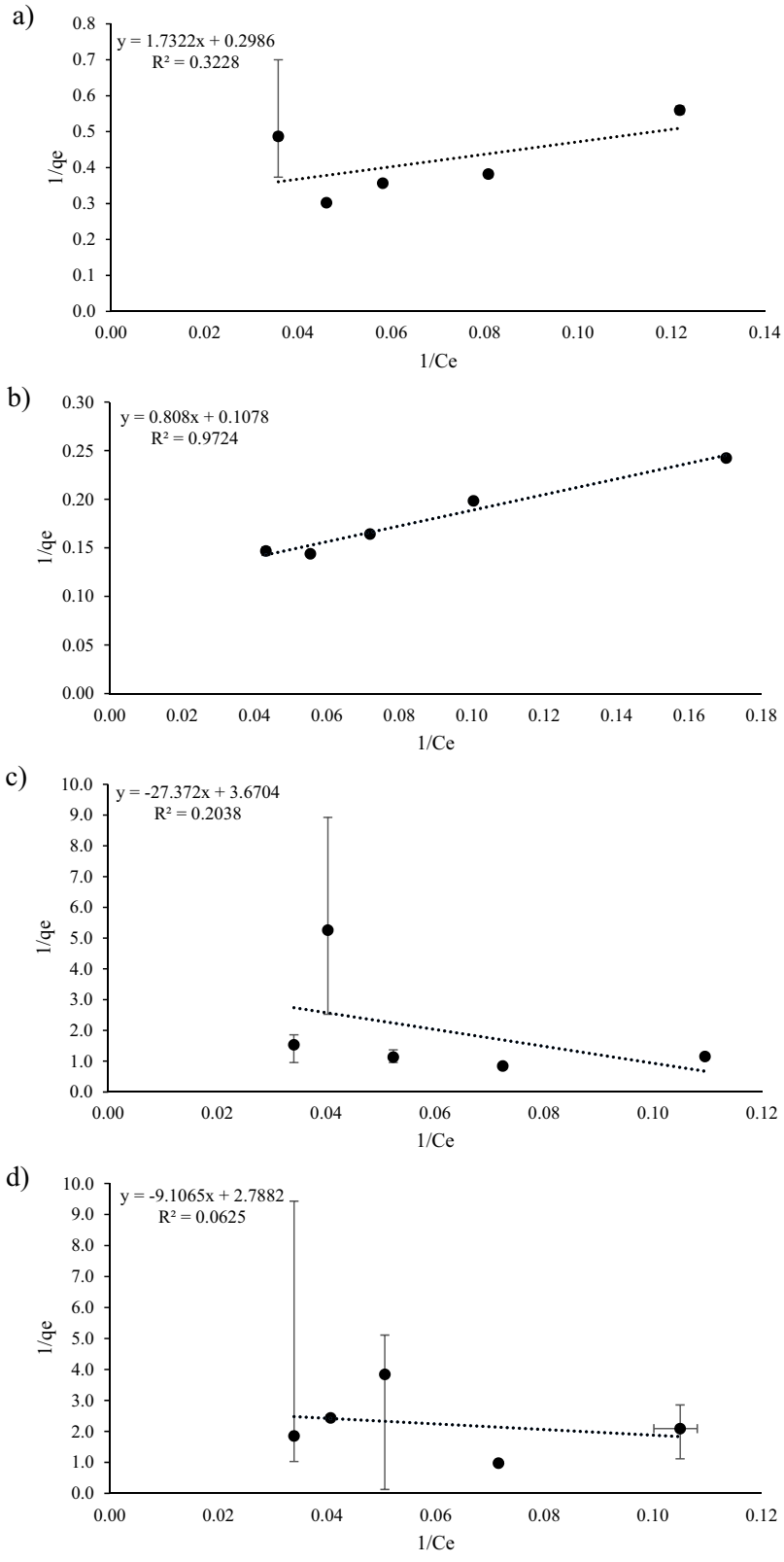

Figure 7: Isotherm Langmuir: (a) O-MAC; (b) M-MAC; (c) Z-AC; and (d) F-MC.

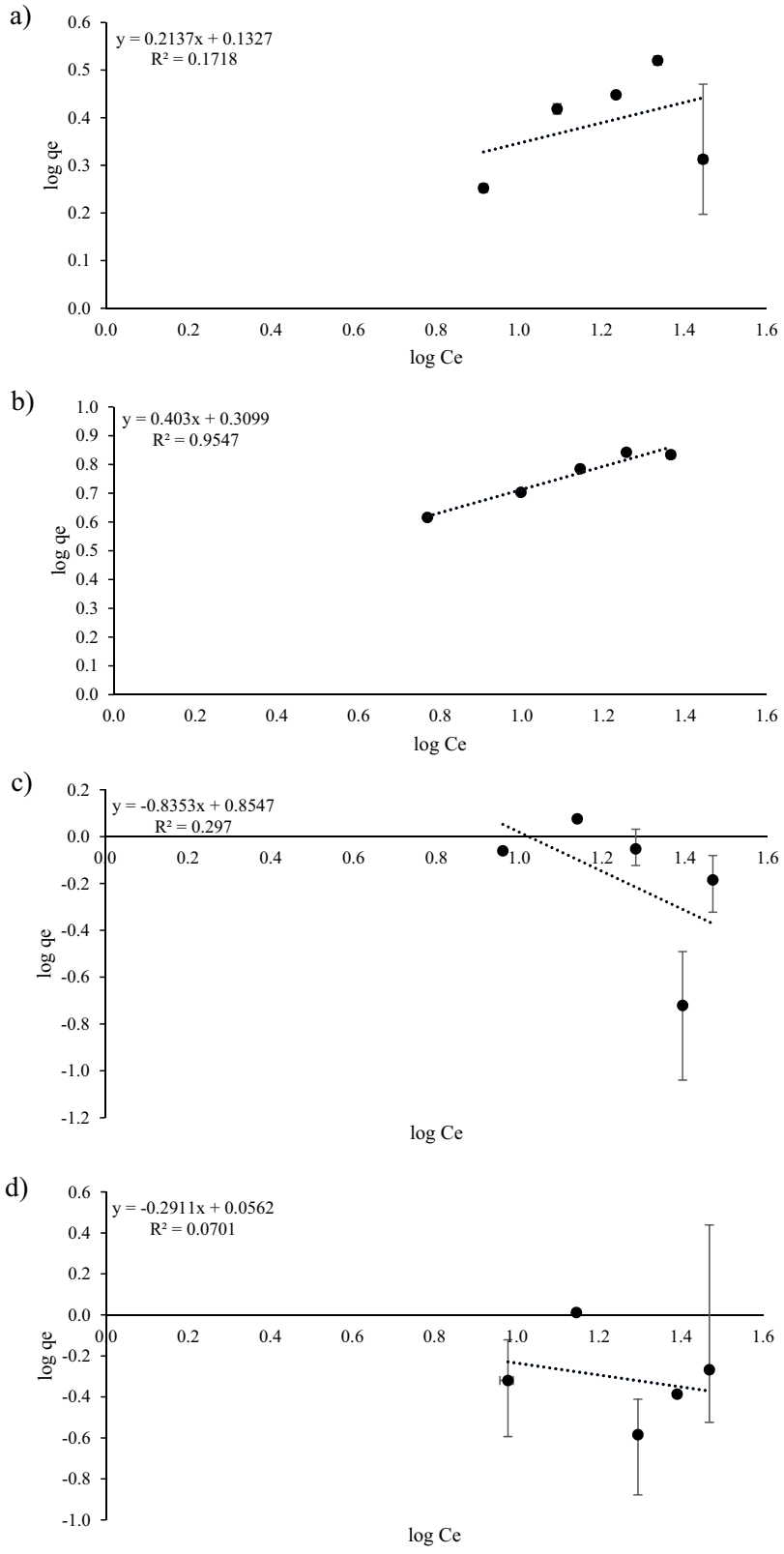

Figure 8: Isotherm Freundlich: (a) O-MAC; (b) M-MAC; (c) Z-AC; and (d) F-MC.

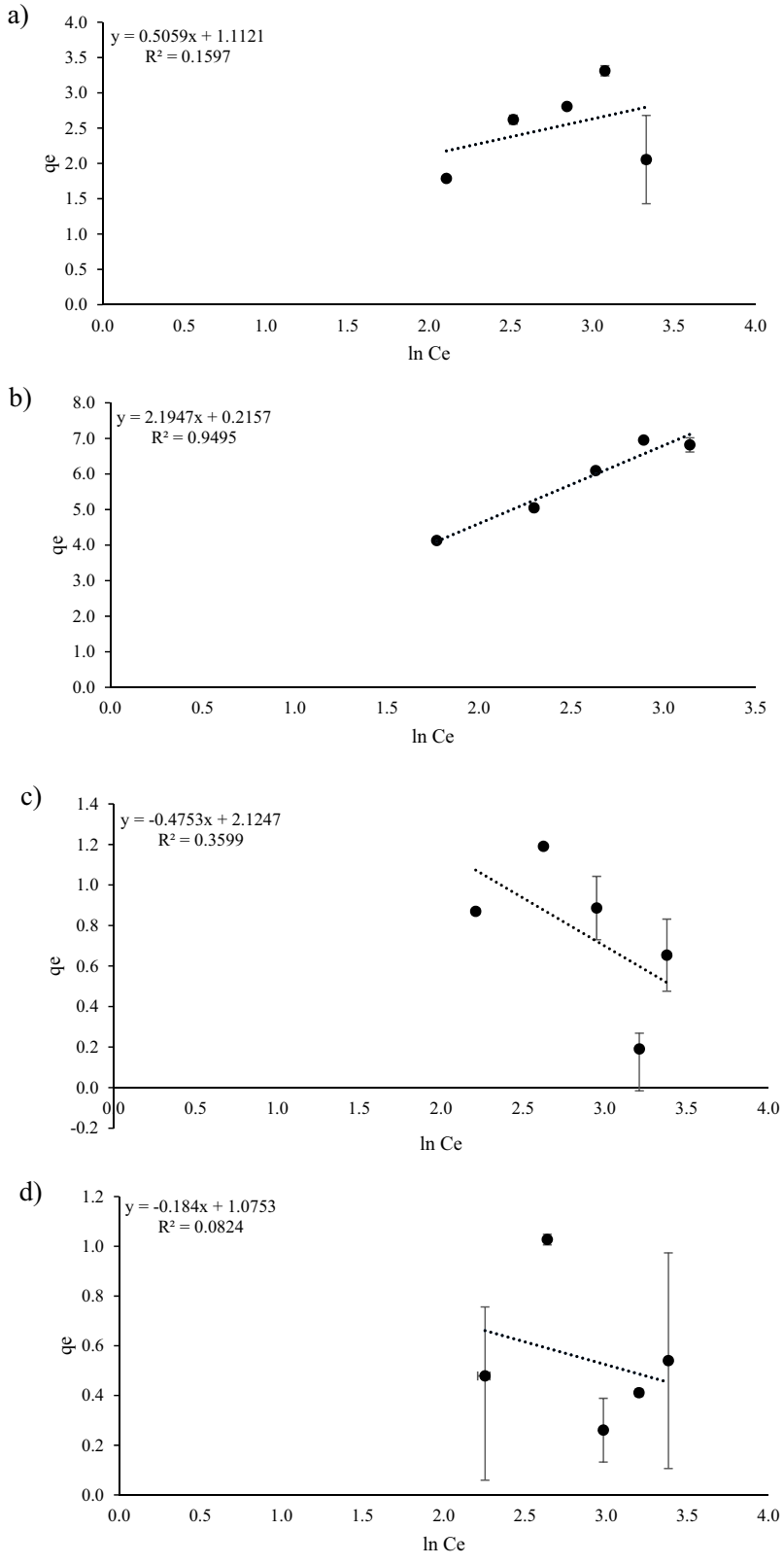

Figure 9: Isotherm Temkin: (a) O-MAC; (b) M-MAC; (c) Z-AC; and (d) F-MC.

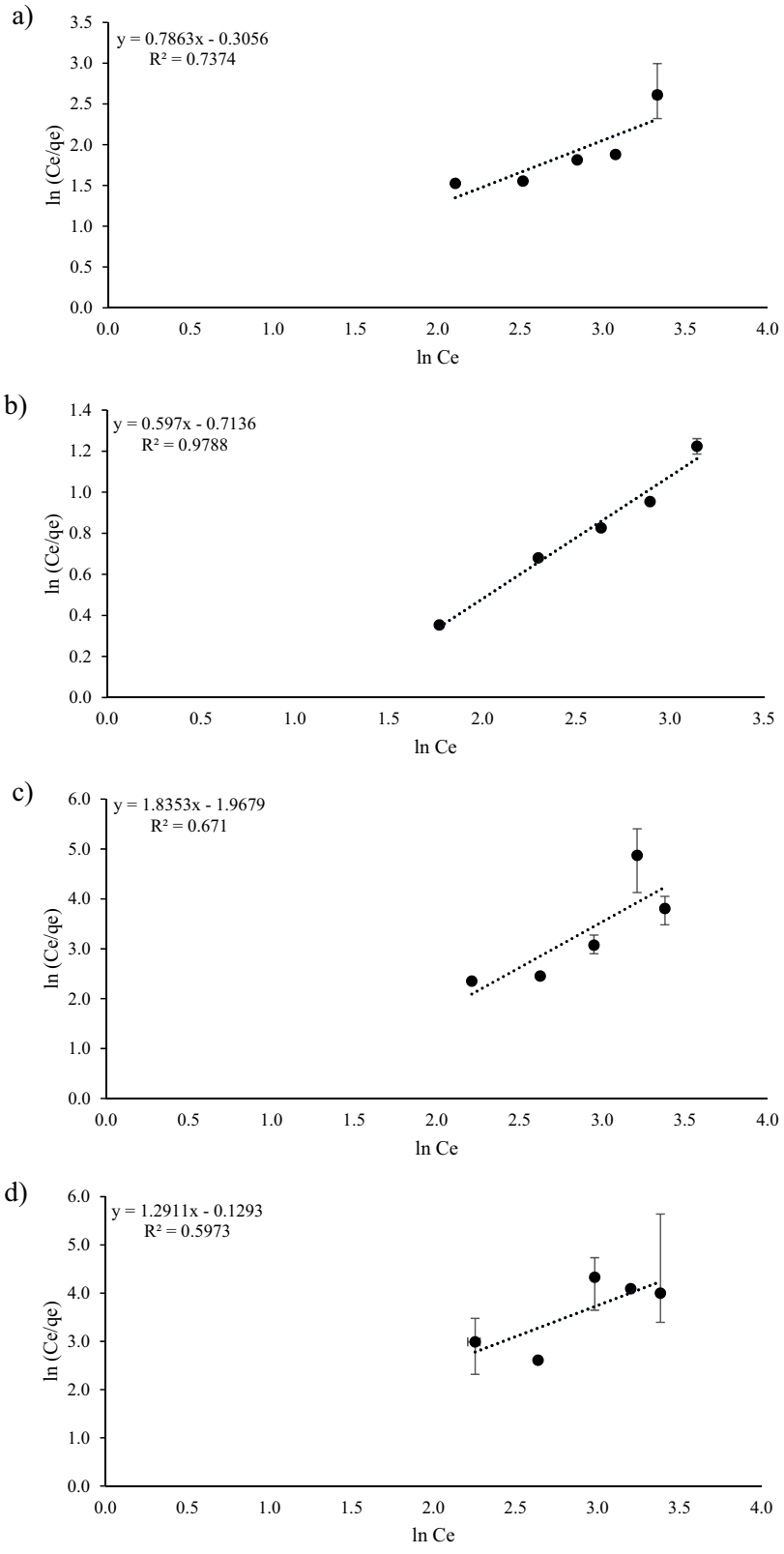

Figure 10: Isotherm Redlich-Peterson: (a) O-MAC; (b) M-MAC; (c) Z-AC; and (d) F-MC.

more uniform surface, consistent with its lower pore uniformity observed in SEM. Notably in Table 2, Z-AC and F-MC exhibited anomalous g values (>1), implying limitations in the model's applicability or competitive adsorption effects, possibly due to their reduced surface areas and pore volumes.

The Langmuir model also performed well for M-MAC (R^2 = 0.9724), supporting monolayer adsorption dominance on its high-surface-area structure. However, Freundlich's poor fit (R^2 = 0.9547 for M-MAC) ruled out purely multilayer adsorption. Temkin's moderate R^2 values (≤0.9495) suggested weaker adsorbent-adsorbate interactions, corroborated by the limited functional group diversity in Z-AC and F-MAC (Figure 2).

These findings align with the BET analysis (Figure 4), where M-MAC's mesoporous structure facilitated higher dye uptake. The Redlich-Peterson model's robustness highlights the coexistence of physical (pore filling) and chemical (π–π/n–π interactions) mechanisms, as depicted in Figure 5. While M-MAC's adsorption aligns with hybrid mechanisms, the single-step samples (O-MAC, Z-AC, F-MC) exhibited less predictable behavior, underscoring the structural advantages of the multi-step synthesis.

3.2.3 Kinetic models

Kinetic models were used to understand the adsorption rate, absorption mechanism, and adsorption efficiency of adsorbents. They also help in analyzing the capacity and mass transfer mechanism of AC. In this study, MAC (1 g·L^{-1}) was introduced into a 10 mg·L^{-1} MO solution, with exposure times ranging from 15 to 180 min. Absorbance was measured using a UV-Vis Spectrophotometer. The study employed pseudo-first-order and pseudo-second-order kinetic models. Figures 11 and 12 illustrated the capacity curves as a function of time and they are compiled in Table 3.

Based on Table 3, the R^2 values for both kinetic models are analyzed. In the pseudo-first-order model, the values for k_1 (adsorption rate) and Q_1 (adsorption capacity) vary greatly among different types of AC. F-MC exhibited the highest adsorption capacity (Q_1 = 19.14 mg·g^{-1}) and an excellent model fit with an R^2 of 0.9486, indicating its suitability for describing F-MC's adsorption process. O-MAC, M-MAC, and Z-AC have lower Q_1 values but still show good model fits based on their determination coefficient (R^2), i.e., 0.6346, 0.9608, and 0.8290, respectively.

Table 2: Isotherm model parameters

Model	Activated carbon			
	O-MAC	M-MAC	Z-AC	F-MC
Langmuir				
Slope (a)	1.7322	0.8080	−27.3720	−9.1065
Intercept (b)	0.2986	0.1078	3.6704	2.7882
q_m	3.3490	9.2764	0.2724	0.3587
K_L	0.1724	0.1334	−0.1341	−0.3062
R^2	0.3228	0.9724	0.2038	0.0625
Freundlich				
Slope (a)	0.2137	0.4030	−0.8353	−0.2911
Intercept (b)	0.1327	−0.6840	0.8547	0.0562
n	4.6795	2.4814	−1.1972	−3.4352
K_F	1.3574	2.0413	7.1565	1.1382
R^2	0.1718	0.9547	0.2970	0.0701
Temkin				
Slope (a)	0.3157	0.4326	−0.7573	−0.4480
Intercept (b)	1.9804	0.0353	3.4496	3.1351
B	26,335.1283	19,218.6778	−10,978.4762	−18,558.0357
ln K_T	6.2730	0.0816	−4.5551	−6.9980
R^2	0.1597	0.9495	0.3599	0.0824
Redlich-Peterson				
Slope (a)	0.7863	0.5970	1.8353	1.2911
Intercept (b)	−0.3056	−0.7163	−1.9679	−0.1293
g	0.7863	0.5970	1.8353	1.2911
K_R	1.3574	2.0468	7.1556	1.1380
R^2	0.7374	0.9788	0.6710	0.5973

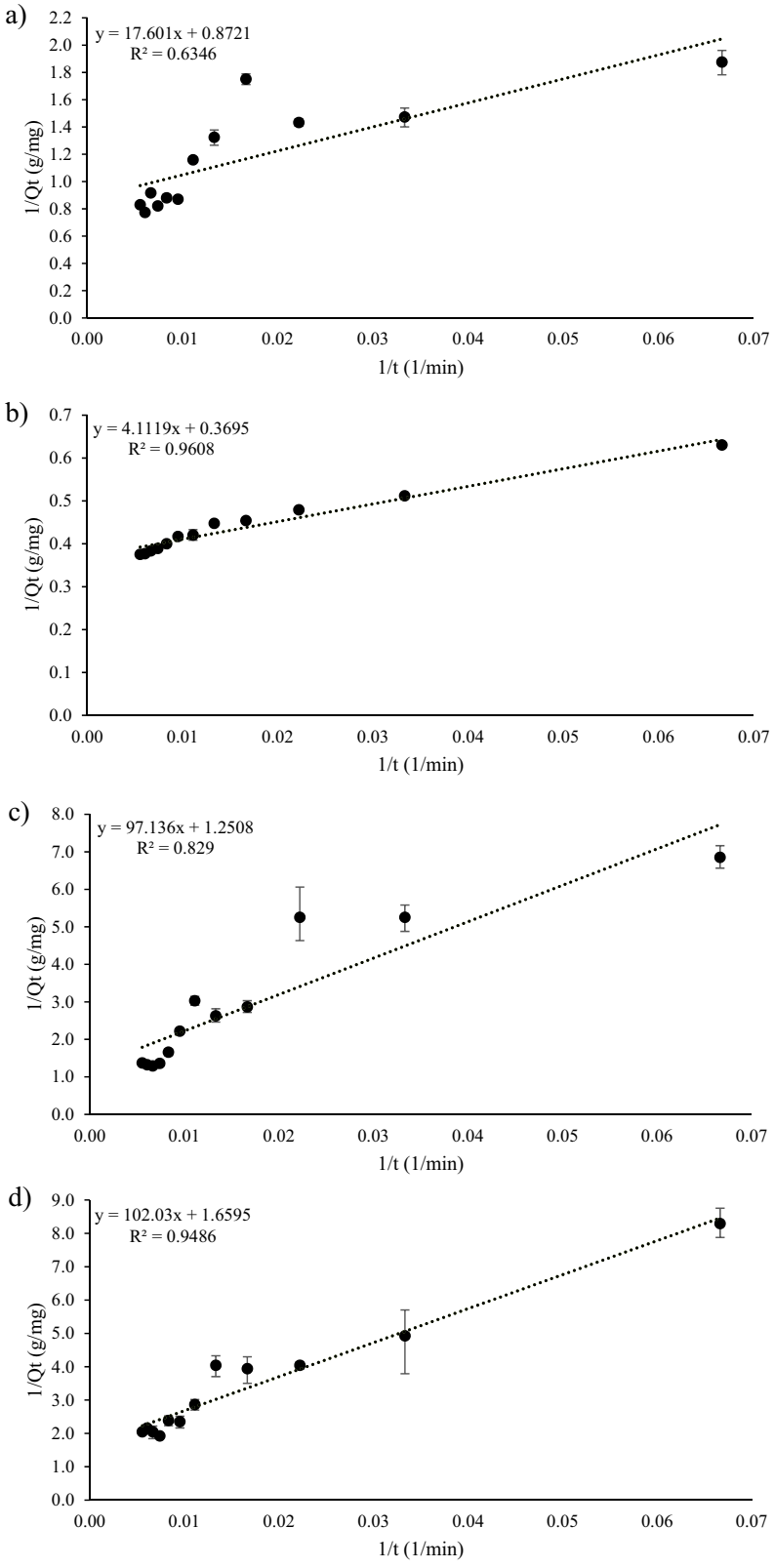

Figure 11: Pseudo first order: (a) O-MAC; (b) M-MAC; (c) Z-AC; and (d) F-MC.

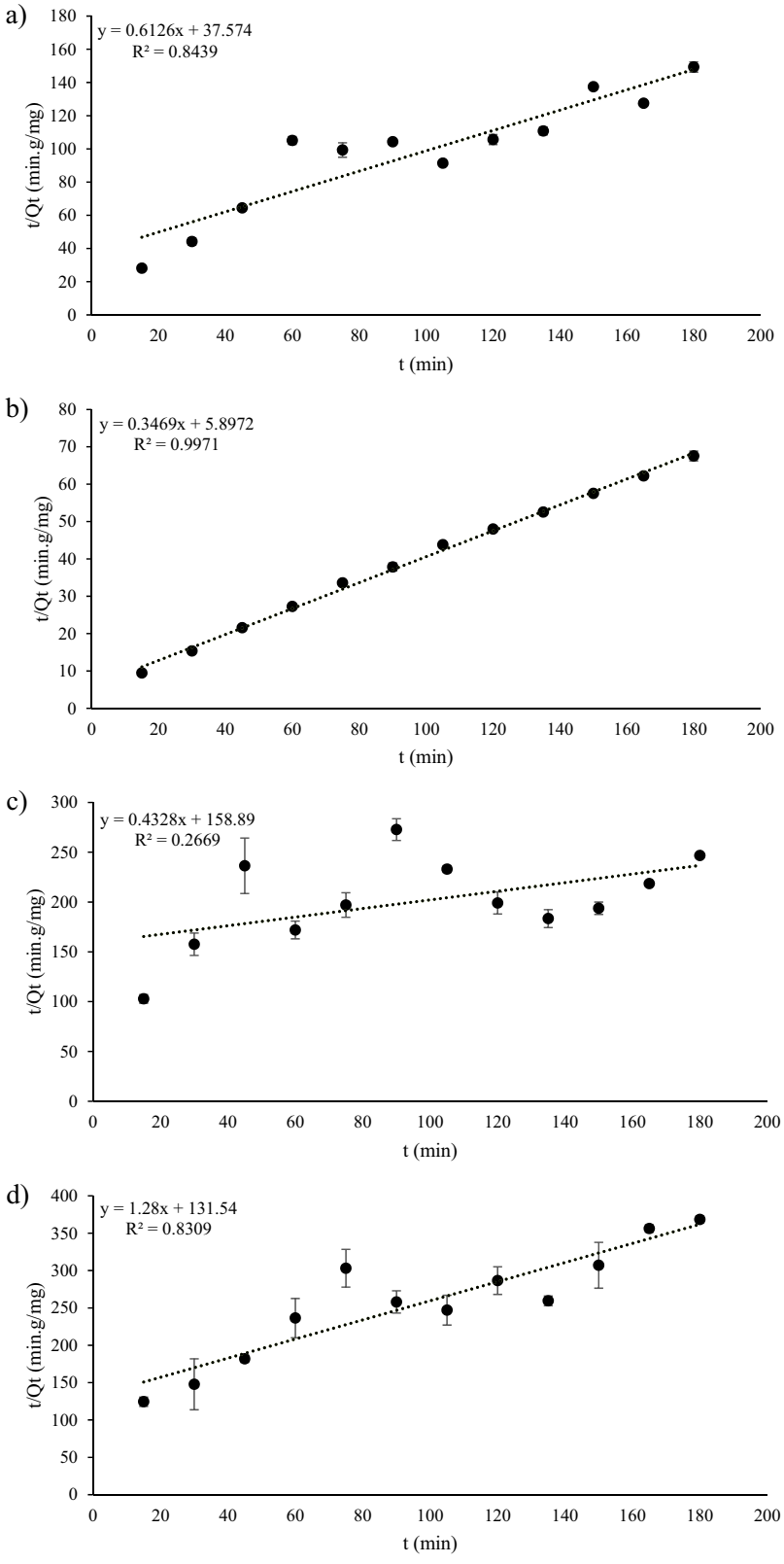

Figure 12: Pseudo second order: (a) O-MAC; (b) M-MAC; (c) Z-AC; and (d) F-MC.

Table 3: Kinetics model parameters

Model	Activated carbon			
	O-MAC	M-MAC	Z-AC	F-MC
Pseudo first order				
Slope (a)	17.6011	4.1119	97.1360	102.0286
Intercept (b)	0.8721	0.3695	1.2508	1.6595
k_1 (1/min)	20.1826	11.1283	77.6567	1952.4021
Q_1 (mg·g^{-1})	1.1467	2.7064	0.7995	19.1358
R^2	0.6346	0.9608	0.8290	0.9486
Pseudo second order				
Slope (a)	0.6126	0.3469	0.4328	1.2800
Intercept (b)	37.5740	5.8972	158.8900	131.5400
k_2 (g·mg^{-1}·min^{-1})	0.0100	0.0204	0.0012	0.00002
Q_2 (mg·g^{-1})	1.6324	2.8827	2.3105	21.1417
R^2	0.8439	0.9971	0.2669	0.8309

In the pseudo-second-order model, the k_2 (adsorption rate) and Q_2 (adsorption capacity) parameters describe the adsorption kinetics. Table 3 shows that M-MAC has the highest k_2 value of 0.0204 g·(mg^{-1}·min^{-1}). Moreover, M-MAC has an adsorption capacity Q_2 of 2.8827 mg·g^{-1} and a very high R^2 value (0.9971), suggesting that the pseudo-second-order model is very suitable for describing M-MAC's adsorption kinetics. O-MAC and F-MC have lower Q_2 values but still show good model fits with R^2 values of 0.8439 for O-MAC and 0.8309 for F-MC. However, Z-AC has a low k_2 value of 0.0012 g·(mg^{-1}·min^{-1}) and a low R^2 value (0.2669), indicating that this model is less suitable for Z-AC.

The differing fits between the pseudo-first-order and pseudo-second-order models suggest distinct adsorption mechanisms for each adsorbent. M-MAC showed a good fit with high R^2 values in both models, but the pseudo-second-order model fits better, indicating more complex physical and chemical interactions. In contrast, the low fit for Z-AC suggests that its adsorption mechanism is more complex and not fully explained by these models. The differences in kinetic model fit are due to the properties of the adsorbate and adsorbent. If the interaction between adsorbate molecules and active sites on the AC is weak or if external diffusion (movement toward the adsorbent surface) dominates over internal diffusion (movement within the adsorbent pores), the pseudo-first-order model may be more appropriate.

3.2.4 Regeneration and reuse study

The regeneration process is essential in determining the durability of MAC. M-MAC, the top-performing AC, was selected to assess its regeneration ability. The regeneration process started with the desorption of used-M-MAC using NaOH as the regenerating agent. The desorption of MO molecules from the solution involved two steps. Initially, the MO molecules adsorbed on the M-MAC surface are replaced by NaOH molecules and then dissolved in the solvent. Subsequently, the adsorbed solvent molecules hinder the interaction between the adsorbent and dye molecules to some extent. According to Table 4, desorption efficiency is higher at rich concentrations of NaOH, achieving 98.34% efficiency for 0.5 mol·L^{-1} and 86.53% for 1 mol·L^{-1}.

Table 4: Effect of NaOH concentration on the M-MAC regeneration

NaOH Conc.	0.5 mol·L^{-1} (%)	1 mol·L^{-1} (%)
% Desorption	93.58	86.53
	98.34	84.59

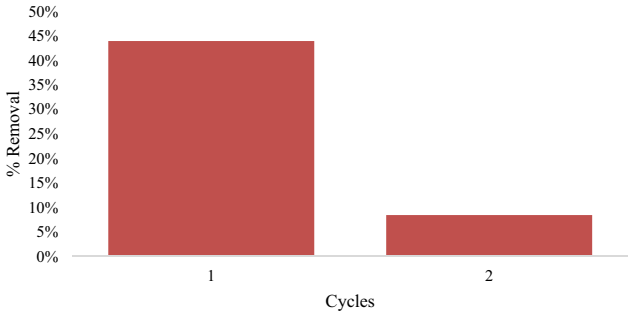

Figure 13: M-MAC regeneration study.

Figure 13 shows the removal process of MO molecules over two cycles. In the first cycle, M-MAC achieves a removal efficiency of 43.93%, which is over 40%. In the second cycle, the efficiency decreases significantly to 8.45%. The test results reveal that the adsorption capacity diminishes with each cycle. This reduction was attributed to some MO molecules not being desorbed from the adsorbent surface during regeneration, rendering some active sites unavailable for adsorption in the following cycles. The effectiveness of NaOH in regenerating MAC has been supported by various studies. For instance, a study has demonstrated that the choice of regenerating agent, mixing time, and concentration play a pivotal role in the desorption process, influencing both the efficiency and longevity of AC adsorbents [54,55].

3.2.5 Comparative analysis to prior studies

A comparative analysis of contaminant uptake efficiency across various adsorbent materials, as documented in

Table 5: Adsorption capacities (q_m) of different adsorbents for MO dye adsorption

Adsorbents	Co ($mg·L^{-1}$)	q_m ($mg·g^{-1}$)	R^2	Ref.
Polyamide 6	5–40	11.16	0.988	[56]
Polyamide 66	5–40	8.85	0.994	[56]
PE+ polyethylene glycol	10	0.78	0.999	[57]
Halloysite nanotubes	10–400	13.56	0.005	[58]
Chrysotile nanotubes	10–600	31.46	0.994	[58]
Activated carbon	20–200	12.76	0.783	[59]
Mesoporous titania nanocomposite	10	2.49	0.999	[60]
Waste tire activated carbon	40–50	9.57	0.990	[61]
Co–Fe layered double hydroxides	20–45	9.19	0.931	[62]
M-MAC	10–30	9.28	0.972	This study

prior research (Table 5), highlights the superior monolayer adsorption capacity (q_m, $mg·g^{-1}$) of the MAC for MO dye removal relative to alternatives. This disparity in performance arises from variations in physicochemical properties, such as porosity, surface reactivity, and functional group composition, which govern adsorption dynamics. While cost-effective options derived from agricultural byproducts, industrial residues, or naturally abundant substrates are widely accessible, their efficacy is often limited without structural or chemical enhancement. Engineered materials, including AC, demonstrate improved contaminant affinity, though their performance hinges on precursor composition, synthesis methodology, and post-treatment modifications.

4 Conclusion

In this study, the PKS has been successfully synthesized into O-MAC, M-MAC, Z-AC, and F-MC using $ZnCl_2$ as the activator and magnetized with $FeCl_3$ using single- and multi-step methods. The multi-step method resulted in larger pore sizes for the MAC compared to the single-step method. Based on FTIR analysis, hydroxyl and carboxyl groups were present in all ACs, indicating that all samples have good adsorption potential. The identification of XRD peaks indicate that MAC was successfully synthesized and adhered to the Fe_3O_4's peak. The BET analysis showed that the magnetic properties of the samples do not affect the adsorption mechanism, significantly.

MAC was also applied for MO adsorption, based on the experiment, O-MAC, M-MAC, Z-AC, and F-MC possessed different maximum adsorption capacities, i.e., 3.3, 6.9, 1.2, and 1.0 $mg·g^{-1}$, respectively, and up to 41% of MO removal. The absorbance test results for MO dye showed a maximum wavelength of 464 nm. Using varying concentrations of MO, the Redlich-Peterson model was found suitable to model the adsorption process for the different types of AC tested. The same process revealed different adsorption kinetics: pseudo-first-order for Z-AC and F-MC and pseudo-second-order for O-MAC and M-MAC. Additionally, M-MAC demonstrated good conformity with high R^2 values in both models. In the regeneration test of M-MAC using NaOH as the regenerating agent, 0.5 $mol·L^{-1}$ NaOH showed higher efficiency than 1 $mol·L^{-1}$ NaOH, with percentages reaching 98.34% for 0.5 $mol·L^{-1}$ and 86.53% for 1 $mol·L^{-1}$. The MO removal was conducted in two cycles with removal percentages of 43.93% and 8.45%. These findings indicate that further development to optimize adsorption applications, regeneration, and reuse studies are still necessary. The study concluded that the multi-step method provides better performance than the single-step method, although it requires more time and resources. Future studies are encouraged to optimize the study through a statistical approach and evaluate the economic feasibility and scalability of these materials, which will be crucial for their practical application in upscale settings.

Acknowledgements: The funding for this initiative was granted via Regular Fundamental Research (*Penelitian Fundamental Reguler*) Directorate General of Higher Education, Research, and Technology: 086/E5/PG.02.00/PL/2024 and 1076.1/UN27.22/PT.01.03/2024.

Funding information: Directorate General of Higher Education, Research, and Technology: 086/E5/PG.02.00/PL/2024 and 1076.1/UN27.22/PT.01.03/2024.

Author contributions: Joko Waluyo: conceptualization, funding acquisition, and supervision; Farida Rahmawati: formal analysis, investigation, methodology, and writing – original draft; Muhammad Izzulhaq: formal analysis, investigation, methodology, visualization, and writing – original

draft; Ibnu Purba: project administration, resources, visualization, and writing – review and editing; Mujtahid Kaavessina: data curation, validation, and writing – review and editing; Wusana Wibowo: resources; Sunu Pranolo: data curation, validation and writing – review and editing; Haris Buwono: validation and writing – review and editing; Ardie Septian: validation and writing – review and editing; Muflih Adnan: validation and writing – review and editing.

Conflict of interest: The authors state no conflict of interest.

Data availability statement: The datasets generated during and/or analyzed during the current study are available from the corresponding author upon reasonable request.

References

[1] Jamee R, Siddique R. Biodegradation of synthetic dyes of textile effluent by microorganisms: an environmentally and economically sustainable approach. Eur J Microbiol Immunol (Bp). 2019;9:114–8.

[2] Pandey A, Pathak VM, Navneet, Rajput M. A feasible approach for azo-dye (methyl orange) degradation by textile effluent isolate Serratia marcescens ED1 strain for water sustainability: AST identification, degradation optimization and pathway hypothesis. Heliyon. 2024;10:e32339.

[3] Singh GB, Vinayak A, Mudgal G, Kesari KK. Azo dye bioremediation: An interdisciplinary path to sustainable fashion. Env Technol Innov. 2024;36:103832.

[4] Serban GV, Iancu VI, Dinu C, Tenea A, Vasilache N, Cristea I, et al. Removal efficiency and adsorption kinetics of methyl orange from wastewater by commercial activated carbon. Sustainability. 2023;15:12939.

[5] Nascimento VX, Schnorr C, Lütke SF, Da Silva M, Machado Machado F, Thue PS, et al. Adsorptive features of magnetic activated carbons prepared by a one-step process towards brilliant blue dye. Molecules. 2023;28:1821.

[6] Sudan S, Kaushal J, Khajuria A. Efficient adsorption of anionic dye (congo red) using copper-carbon dots doped magnetic biochar: kinetic, isothermal, and regeneration studies. Clean Technol Env Policy. 2024;26:481–97.

[7] Zhang S, Tao L, Jiang M, Gou G, Zhou Z. Single-step synthesis of magnetic activated carbon from peanut shell. Mater Lett. 2015;157:281–4.

[8] Nguyen HM, Tran AT, Nguyen DNL, Lam HH, Tran-Thuy TM, Nguyen LQ, et al. One-pot fabrication of zero-valent iron-embedded activated carbon from rosemary distillation residues for malachite green removal. Mater Res Express. 2023;10:085603.

[9] Demarchi CA, Michel BS, Nedelko N, Ślawska-Waniewska A, Dłużewski P, Kaleta A, et al. Preparation, characterization, and application of magnetic activated carbon from termite feces for the adsorption of Cr(VI) from aqueous solutions. Powder Technol. 2019;354:432–41.

[10] Zhang X, Li Y, He Y, Kong D, Klein B, Yin S, et al. Preparation of magnetic activated carbon by activation and modification of char derived from co-pyrolysis of lignite and biomass and its adsorption of heavy-metal-containing wastewater. Minerals. 2022;12:665.

[11] Duan Z, Zhang W, Lu M, Shao Z, Huang W, Li J, et al. Magnetic Fe_3O_4/activated carbon for combined adsorption and Fenton oxidation of 4-chlorophenol. Carbon N Y. 2020;167:351–63.

[12] Jiang Y, Xie Q, Zhang Y, Geng C, Yu B, Chi J. Preparation of magnetically separable mesoporous activated carbons from brown coal with Fe_3O_4. Int J Min Sci Technol. 2019;29:513–9.

[13] Zhang Z, Wang T, Zhang H, Liu Y, Xing B. Adsorption of Pb(II) and Cd(II) by magnetic activated carbon and its mechanism. Sci Total Env. 2021;757:143910.

[14] Rattanapan S, Srikram J, Kongsune P. Adsorption of methyl orange on coffee grounds activated carbon. Energy Procedia. 2017;138:949–54.

[15] Fu J, Kang Q, Ao W, Wahab N, Mao X, Ran C, et al. Comparison and analysis of one- and two-step activation for preparation of activated carbon from furfural residues. Biomass Convers Biorefin. 2023;13:4681–94.

[16] Lee LZ, Ahmad Zaini MA. One-step $ZnCl_2$/$FeCl_3$ composites preparation of magnetic activated carbon for effective adsorption of rhodamine B dye. Toxin Rev. 2022;41:64–81.

[17] Kittappa S, Jais FM, Ramalingam M, Mohd NS, Ibrahim S. Functionalized magnetic mesoporous palm shell activated carbon for enhanced removal of azo dyes. J Env Chem Eng. 2020;8:104081.

[18] Anyika C, Asri NAM, Majid ZA, Jaafar J, Yahya A. Batch sorption–desorption of As(III) from waste water by magnetic palm kernel shell activated carbon using optimized Box–Behnken design. Appl Water Sci. 2017;7:4573–91.

[19] Ambarita H, Kawai H. Utilization of renewable and conventional energy in palm oil industry in Indonesia. IOP Conf Ser Earth Env Sci. 2021;753:012002.

[20] Lam WY, Kulak M, Sim S, King H, Huijbregts M, Chaplin-Kramer R. Greenhouse gas footprints of palm oil production in Indonesia over space and time. Sci Total Env. 2019;688:827–37.

[21] Waluyo J, Makertihartha IG, Susanto H. Pyrolysis with intermediate heating rate of palm kernel shells: Effect temperature and catalyst on product distribution. AIP Conf Proc. 2018;1977:20026.

[22] Pranolo SH, Waluyo J, Putro FA, Adnan MA, Kibria MG. Gasification process of palm kernel shell to fuel gas: Pilot-scale experiment and life cycle analysis. Int J Hydrog Energy. 2023;48:2835–48.

[23] Waluyo J, Ruya PM, Hantoko D, Rizkiana J, Makertihartha IGBN, Yan M, et al. Utilization of modified zeolite as catalyst for steam gasification of palm kernel shell. Bull Chem React Eng Catal. 2021;16:623–31.

[24] Wang Q, Zhang Y, Zheng Y, Fagbohun EO, Cui Y. Magnetic activated carbon for the removal of methyl orange from water via adsorption and Fenton-like degradation. Particuology. 2024;94:314–26.

[25] Li Y, Zimmerman AR, He F, Chen J, Han L, Chen H, et al. Solvent-free synthesis of magnetic biochar and activated carbon through ball-mill extrusion with Fe_3O_4 nanoparticles for enhancing adsorption of methylene blue. Sci Total Env. 2020;722:137972.

[26] Costa F, di Summa PG, Srinivasan J. Low-cost magnetic activated carbon with excellent capacity for organic adsorption obtained by a novel synthesis route. J Env Chem Eng. 2021;9:105061.

[27] Astuti W, Sulistyaningsih T, Kusumastuti E, Thomas G, Kusnadi RY. Thermal conversion of pineapple crown leaf waste to magnetized activated carbon for dye removal. Bioresour Technol. 2019;287:121426.

[28] Wen Y, Zheng Z, Wang S, Han T, Yang W, Jönsson PG. Magnetic bio-activated carbons production using different process parameters

for phosphorus removal from artificially prepared phosphorus-rich and domestic wastewater. Chemosphere. 2021;271:129561.
[29] Illingworth JM, Rand B, Williams PT. Understanding the mechanism of two-step, pyrolysis-alkali chemical activation of fibrous biomass for the production of activated carbon fibre matting. Fuel Process Technol. 2022;235:107348.
[30] Contreras RR, Almarza J, Rincón L, Ruiz C. Green sodium hydroxide for industrial purposes. A short review. J Env Chem Eng. 2025;13:114972.
[31] Sithole T. A review on regeneration of adsorbent and recovery of metals: Adsorbent disposal and regeneration mechanism. S Afr J Chem Eng. 2024;50:39–50.
[32] Rasouli Sadabad H, Coleman HM, Dooley JSG, Snelling WJ, O'Hagan B, Ganin AY, et al. Desorption of antibiotics from granular activated carbon during water treatment by adsorption. Env Process. 2024;11:1–27.
[33] El Messaoudi N, El Khomri M, Chlif N, Chegini ZG, Dbik A, Bentahar S, et al. Desorption of Congo red from dye-loaded Phoenix dactylifera date stones and Ziziphus lotus jujube shells. Groundw Sustain Dev. 2021;12:100552.
[34] Zhi LL, Zaini MAA. One-step synthesis of magnetic activated carbons for methylene blue dye removal: activation conditions and adsorption studies. Desalin Water Treat. 2020;198:434–44.
[35] Wei F, Jin S, Yao C, Wang T, Zhu S, Ma Y, et al. Revealing the combined effect of active sites and intra-particle diffusion on adsorption mechanism of methylene blue on activated red-pulp pomelo peel biochar. Molecules. 2023;28:4426.
[36] Al-Ghouti MA, Da'ana DA. Guidelines for the use and interpretation of adsorption isotherm models: A review. J Hazard Mater. 2020;393:122383.
[37] Somsesta N, Sricharoenchaikul V, Aht-Ong D. Adsorption removal of methylene blue onto activated carbon/cellulose biocomposite films: Equilibrium and kinetic studies. Mater Chem Phys. 2020;240:122221.
[38] Namikuchi EA, Gaspar RDL, Da Silva DS, Raimundo IM, Mazali IO. PEG size effect and its interaction with Fe_3O_4 nanoparticles synthesized by solvothermal method: morphology and effect of pH on the stability. Nano Express. 2021;2:020022.
[39] Nguyen DV, Nguyen HM, Bui Q, Do T, Lam HH, Tran-Thuy TM, et al. Magnetic activated carbon from $ZnCl_2$ and $FeCl_3$ coactivation of lotus seedpod: One-pot preparation, characterization, and catalytic activity towards robust degradation of acid orange 10. Bioinorg Chem Appl. 2023;2023:3848456.
[40] Łoński S, Łukowiec D, Barbusiński K, Babilas R, Szeląg B, Radoń A. Flower-like magnetite nanoparticles with unfunctionalized surface as an efficient catalyst in photo-Fenton degradation of chemical dyes. Appl Surf Sci. 2023;638:158127.
[41] Mohammadifard A, Allouss D, Vosoughi M, Dargahi A, Moharrami A. Synthesis of magnetic Fe_3O_4/activated carbon prepared from banana peel (BPAC@Fe_3O_4) and salvia seed (SSAC@Fe_3O_4) and applications in the adsorption of Basic Blue 41 textile dye from aqueous solutions. Appl Water Sci. 2022;12:1–11.
[42] Singh S, Mandal M, Mishra T, Angayarkanni A, Veldurthi NK, Pati SS. Facile synthesis of citric acid functionalized Fe_3O_4@activated carbon magnetic nanocomposite for efficient adsorption of brilliant green dye from wastewater. ChemistrySelect. 2023;8:e202205045.
[43] Ren J, Weng H, Li B, Chen F, Liu J, Song Z. The influence mechanism of pore structure of tectonically deformed coal on the adsorption and desorption hysteresis. Front Earth Sci (Lausanne). 2022;10:841353.
[44] Qi L, Zhou X, Peng X, Chen X, Wang Z, Dai J. A study on the pore structure and fractal characteristics of briquettes with different compression loads. Sustainability. 2022;14:12148.
[45] Zhang Q, Cheng Y, Fang C, Chen J, Chen H, Li H, et al. Facile synthesis of porous carbon/Fe3O4 composites derived from waste cellulose acetate by one-step carbothermal method as a recyclable adsorbent for dyes. J Mater Res Technol. 2020;9:3384–93.
[46] Hamid Y, Kanti Sen T. Application of synthesized biomass bamboo charcoal–iron oxide "BC/Fe" nanocomposite adsorbents in the removal of cationic methylene blue dye contaminants from wastewater by adsorption. Sustainability. 2023;15:8841.
[47] Dominguez M, Mendoza J, Figueroa K. Adsorption of methylene blue dye using common walnut shell (Juglans regia) like biosorbent: implications for wastewater treatment. Green Chem Lett Rev. 2024;17(1):2362257.
[48] Benalia A, Derbal K, Baatache O, Lehchili C, Khalfaoui A, Pizzi A. Removal of dyes from water using aluminum-based water treatment sludge as a low-cost coagulant: use of response surface methodology. Water. 2024;16:1400.
[49] Hoong HNJ, Ismail N. Removal of dye in wastewater by adsorption-coagulation combined system with hibiscus sabdariffa as the coagulant. MATEC Web Conf. 2018;152:01008.
[50] Elzahar MMH, Bassyouni M. Removal of direct dyes from wastewater using chitosan and polyacrylamide blends. Sci Rep. 2023;13(1):1–16.
[51] Bożęcka A, Orlof-Naturalna M, Kopeć M. Methods of dyes removal from aqueous environment. J Ecol Eng. 2021;22:111–8.
[52] Xie Z, Diao S, Xu R, Wei G, Wen J, Hu G, et al. Effective removal of dyes from wastewater by Osmanthus fragrans biomass charcoal. Molecules. 2023;28:6305.
[53] Mirzaee E, Sartaj M. Activated carbon-based magnetic composite as an adsorbent for removal of polycyclic aromatic hydrocarbons from aqueous phase: Characterization, adsorption kinetics and isotherm studies. J Hazard Mater Adv. 2022;6:100083.
[54] Shu Q, Legrand L, Kuntke P, Tedesco M, Hamelers H. Electrochemical regeneration of spent alkaline absorbent from direct air capture. Env Sci Technol. 2020;54:8990–8.
[55] Ding H, Zhu Y, Wu Y, Zhang J, Deng H, Zheng H, et al. In situ regeneration of phenol-saturated activated carbon fiber by an electro-peroxymonosulfate process. Env Sci Technol. 2020;54:10944–53.
[56] Wang K, Kou Y, Wang K, Liang S, Guo C, Wang W, et al. Comparing the adsorption of methyl orange and malachite green on similar yet distinct polyamide microplastics: Uncovering hydrogen bond interactions. Chemosphere. 2023;340:139806.
[57] Hanif MA, Ibrahim N, Dahalan FA, Md Ali UF, Hasan M, Azhari AW, et al. Microplastics in facial cleanser: extraction, identification, potential toxicity, and continuous-flow removal using agricultural waste–based biochar. Env Sci Pollut Res Int. 2023;30:60106–20.
[58] Wu L, Liu X, Lv G, Zhu R, Tian L, Liu M, et al. Study on the adsorption properties of methyl orange by natural one-dimensional nano-mineral materials with different structures. Sci Rep. 2021;11:1–11.
[59] Abu al-Rub SS, Alyami BA, Alqahtani YS, Alqarih AR, Dunquwah BA, Alyami MM, et al. Comparative adsorption of methyl orange color from an aqueous solution using activated carbon. Indian J Pharm Educ Res. 2024;58:679–84.

[60] Gao L, Zhang Q, Li J, Feng R, Xu H, Xue C. Adsorption of methyl orange on magnetically separable mesoporous titania nanocomposite. Chin J Chem Eng. 2014;22:1168–73.
[61] Khan TA, Rahman R, Khan EA. Adsorption of malachite green and methyl orange onto waste tyre activated carbon using batch and fixed-bed techniques: isotherm and kinetics modeling. Model Earth Syst Env. 2017;3:1–14.
[62] Xie YL, Ye FP, Zhao SQ. Preparation of magnetic Co–Fe layered double hydroxides and its adsorption properties for the removal of methyl orange. J Chem Res. 2023;47(1):1–8.